JACS
JOURNAL OF THE AMERICAN CHEMICAL SOCIETY

ARTICLE

pubs.acs.org/JACS

Doping Metal−Organic Frameworks for Water Oxidation, Carbon Dioxide Reduction, and Organic Photocatalysis

Cheng Wang, Zhigang Xie, Kathryn E. deKrafft, and Wenbin Lin*

Department of Chemistry, CB #3290, University of North Carolina, Chapel Hill, North Carolina 27599, United States

Supporting Information

ABSTRACT: Catalytically competent Ir, Re, and Ru complexes H_2L_1−H_2L_6 with dicarboxylic acid functionalities were incorporated into a highly stable and porous $Zr_6O_4(OH)_4(bpdc)_6$ (UiO-67, bpdc = *para*-biphenyldicarboxylic acid) framework using a mix-and-match synthetic strategy. The matching ligand lengths between bpdc and L_1−L_6 ligands allowed the construction of highly crystalline UiO-67 frameworks (metal−organic frameworks (MOFs) **1**−**6**) that were doped with L_1−L_6 ligands. MOFs **1**−**6** were isostructural to the parent UiO-67 framework as shown by powder X-ray diffraction (PXRD) and exhibited high surface areas ranging from 1092 to 1497 m^2/g. MOFs **1**−**6** were stable in air up to 400 °C and active catalysts in a range of reactions that are relevant to solar energy utilization. MOFs **1**−**3** containing $[Cp^*Ir^{III}(dcppy)Cl]$ (H_2L_1), $[Cp^*Ir^{III}(dcbpy)Cl]Cl$ (H_2L_2), and $[Ir^{III}(dcppy)_2(H_2O)_2]OTf$ (H_2L_3) (where Cp* is pentamethylcyclopentadienyl, dcppy is 2-phenylpyridine-5,4′-dicarboxylic acid, and dcbpy is 2,2′-bipyridine-5,5′-dicarboxylic acid) were effective water oxidation catalysts (WOCs), with turnover frequencies (TOFs) of up to 4.8 h^{-1}. The $[Re^I(CO)_3(dcbpy)Cl]$ (H_2L_4) derivatized MOF **4** served as an active catalyst for photocatalytic CO_2 reduction with a total turnover number (TON) of 10.9, three times higher than that of the homogeneous complex H_2L_4. MOFs **5** and **6** contained phosphorescent $[Ir^{III}(ppy)_2(dcbpy)]Cl$ (H_2L_5) and $[Ru^{II}(bpy)_2(dcbpy)]Cl_2$ (H_2L_6) (where ppy is 2-phenylpyridine and bpy is 2,2′-bipyridine) and were used in three photocatalytic organic transformations (aza-Henry reaction, aerobic amine coupling, and aerobic oxidation of thioanisole) with very high activities. The inactivity of the parent UiO-67 framework and the reaction supernatants in catalytic water oxidation, CO_2 reduction, and organic transformations indicate both the molecular origin and heterogeneous nature of these catalytic processes. The stability of the doped UiO-67 catalysts under catalytic conditions was also demonstrated by comparing PXRD patterns before and after catalysis. This work illustrates the potential of combining molecular catalysts and MOF structures in developing highly active heterogeneous catalysts for solar energy utilization.

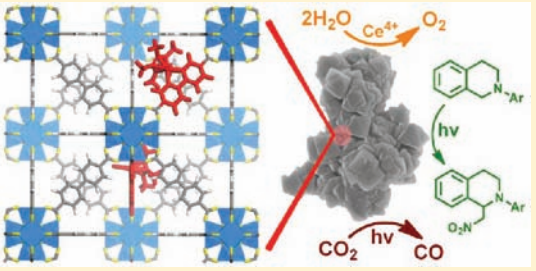

INTRODUCTION

Sunlight provides the most attractive and abundant renewable energy source to meet mankind's future energy needs.[1] Chemists have long been interested in building artificial photosynthetic systems to harvest solar energy and to enable visible-light-driven organic synthesis.[2] Although the first artificial photodriven water splitting was demonstrated with a solid state semiconductor,[3] significant recent efforts have been devoted to exploring molecular systems for energy harvesting, due to the ease of their structure/property tuning. Numerous molecular systems have now been designed to serve as individual functional components in an artificial photosynthetic device. For example, efficient molecular antenna have been constructed from cyclic tetrapyrroles and $[Ru(bpy)_3]^{2+}$ (bpy = 2,2′-bipyridine) or $[Ir(ppy)_2(bpy)]^+$ (ppy = 2-phenylpyridine) derivatives.[4] Molecular catalysts have also been developed for a range of energy-storing reactions, such as water oxidation,[5] hydrogen production,[6,7] and carbon dioxide reduction.[7,8] In addition, molecular phosphors such as $[Ru(bpy)_3]^{2+}$ and $[Ir(ppy)_2(bpy)]^+$ have been used to perform visible-light-driven organic transformations, leading to new mild, clean, and atom-efficient methodologies for organic synthesis.[9]

One of the remaining challenges in artificial synthesis is the integration of individual components in a structurally controlled manner to create an efficient functional device. The photoelectrochemical cell (PEC) provides a promising design which harvests molecular excitations via electron injection into the conduction band of a semiconductor.[4,5] Molecular catalysts attached to the electrode surface then use the separated electrons and holes to drive energy-storing chemical reactions. Self-assembly of large molecules into nano- or microscale structures has also been identified as a potential strategy to achieve an integrated light-harvesting system.[4,10]

Metal−organic frameworks (MOFs) have recently emerged as an interesting class of porous solids that can be constructed from a variety of molecular complexes[11−15] and explored for a range of applications in gas storage,[16,17] compound separation,[18,19] chemical sensing,[20−23] nonlinear optics,[24] biomedical imaging,[25−27]

Received: April 18, 2011
Published: July 22, 2011

Scheme 1. Synthesis of Doped UiO-67

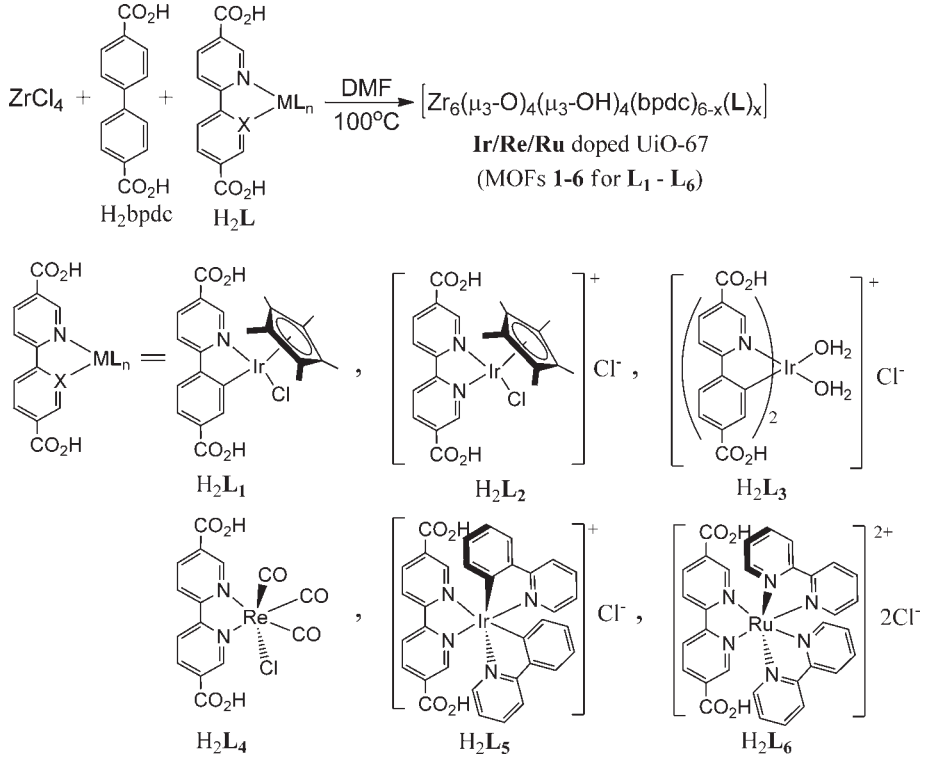

drug delivery,[28−30] and heterogeneous catalysis.[31−35] We are interested in utilizing MOFs as a platform to integrate individual functional components for solar energy harvesting. For example, we recently demonstrated efficient energy migration in Os-doped Ru(II)-bpy MOFs where the Ru(II)* excited states transferred energy to lower-lying (∼0.5 eV) Os(II) trap sites via multiple Ru(II)* → Ru(II) hops.[36] Herein, we report the development of the first MOF-based heterogeneous catalytic systems for water oxidation, photocatalytic CO_2 reduction, and visible light-driven organic photocatalysis.

Catalytic water oxidation constitutes a key half reaction in artificial photosynthesis.[4,5] A large number of homogeneous water oxidation catalysts (WOCs) have recently been developed based on dimeric Ru complexes,[37,38] monomeric Ru and Fe complexes,[39−41] monomeric Ir complexes,[42−44] and polyoxometalates with a Ru_4O_4 or a Co_4O_4 core.[45,46] These molecular WOCs are highly tunable with high catalyst activity and stability. On the other hand, heterogeneous WOCs based on iridium oxide[47−49] and cobalt oxide/phosphate[50,51] particles can be readily interfaced with electrodes or photosensitizers to achieve electrocatalytic or photocatalytic water oxidation. We believe it is beneficial to incorporate the molecular WOCs into framework structures. Unfortunately, most MOF structures tend to lack stability under water oxidation reaction conditions.[52] The UiO family of MOFs based on $Zr_6O_4(OH)_4(CO_2)_{12}$ secondary building units (SBUs) and dicarboxylate bridging ligands represent an interesting exception and is very stable in water.[53,54] We successfully incorporated three iridium-based WOCs, $[Ir^{III}(Cp^*)(dcppy)]$ ($H_2\mathbf{L_1}$, where Cp* = pentamethylcyclopentadienyl, dcppy = 2-phenylpyridine-5,4′-dicarboxylic acid), $[Ir^{III}(Cp^*)(dcbpy)]^+$ (dcbpy = 2,2′-bipyridine-5,5′-dicarboxylic acid) ($H_2\mathbf{L_2}$), and $[Ir^{III}(dcppy)_2(H_2O)]^+$ ($H_2\mathbf{L_3}$), into the $Zr_6O_4(OH)_4(bpdc)_6$ (UiO-67, bpdc = *para*-biphenyldicarboxylate) framework (MOFs **1**−**3**) and demonstrated catalytic water oxidation by these highly stable MOFs.

In photosynthesis, the reducing equivalents resulting from water oxidation reactions in Photosystem II are used to drive CO_2 reduction in Photosystem I.[55] Photochemically reducing CO_2 into a source of fuel offers an attractive way to both harvest energy from sunlight and alleviate the rise of atmospheric CO_2 concentrations.[8] A number of molecular photocatalysts, including cobalt/nickel tetraaza-macrocyclic compounds,[56−60] iron/cobalt metalloporphyrins,[61−65] and $Re^I(CO)_3(bpy)X$ complexes,[66−70] have been examined for CO_2 reduction in recent years. We successfully incorporated $Re^I(CO)_3(dcbpy)Cl$ ($H_2\mathbf{L_4}$) into the UiO-67 framework to afford a heterogeneous photocatalyst for CO_2 reduction using visible light.

Organic transformations driven by visible light are gaining increasing interest from synthetic chemists because of generally mild reaction conditions, atom efficiency, and the potential to mediate thermodynamically uphill reactions.[71] Photocatalysts are often required in visible-light-driven organic reactions since the majority of organic substrates in these reactions do not readily absorb photons in the visible region. $[Ru(bpy)_3]^{2+}$ and $[Ir(ppy)_2(bpy)]^+$ have been reported recently as photoredox catalysts in a variety of new photocatalytic organic reactions, such as [2 + 2] cycloaddition,[72] tin-free dehalogenation,[73] aza-Henry reactions,[74] aerobic amine coupling,[75,76] sulfide and alcohol oxidation,[77,78] olefin epoxidation,[79] functional group transformation,[80] asymmetric organophotoredox catalysis,[81] and radical chemistry.[82] Because these photocatalysts contain precious metals, it is highly desirable to develop recyclable and reusable heterogeneous photocatalytic systems based on molecular phosphors. We incorporated $[Ir^{III}(ppy)_2(dcbpy)]Cl$ ($H_2\mathbf{L_5}$) and $[Ru^{II}(bpy)_2(dcbpy)]Cl_2$ ($H_2\mathbf{L_6}$) into the UiO-67 framework and demonstrated the applications of these doped MOFs as

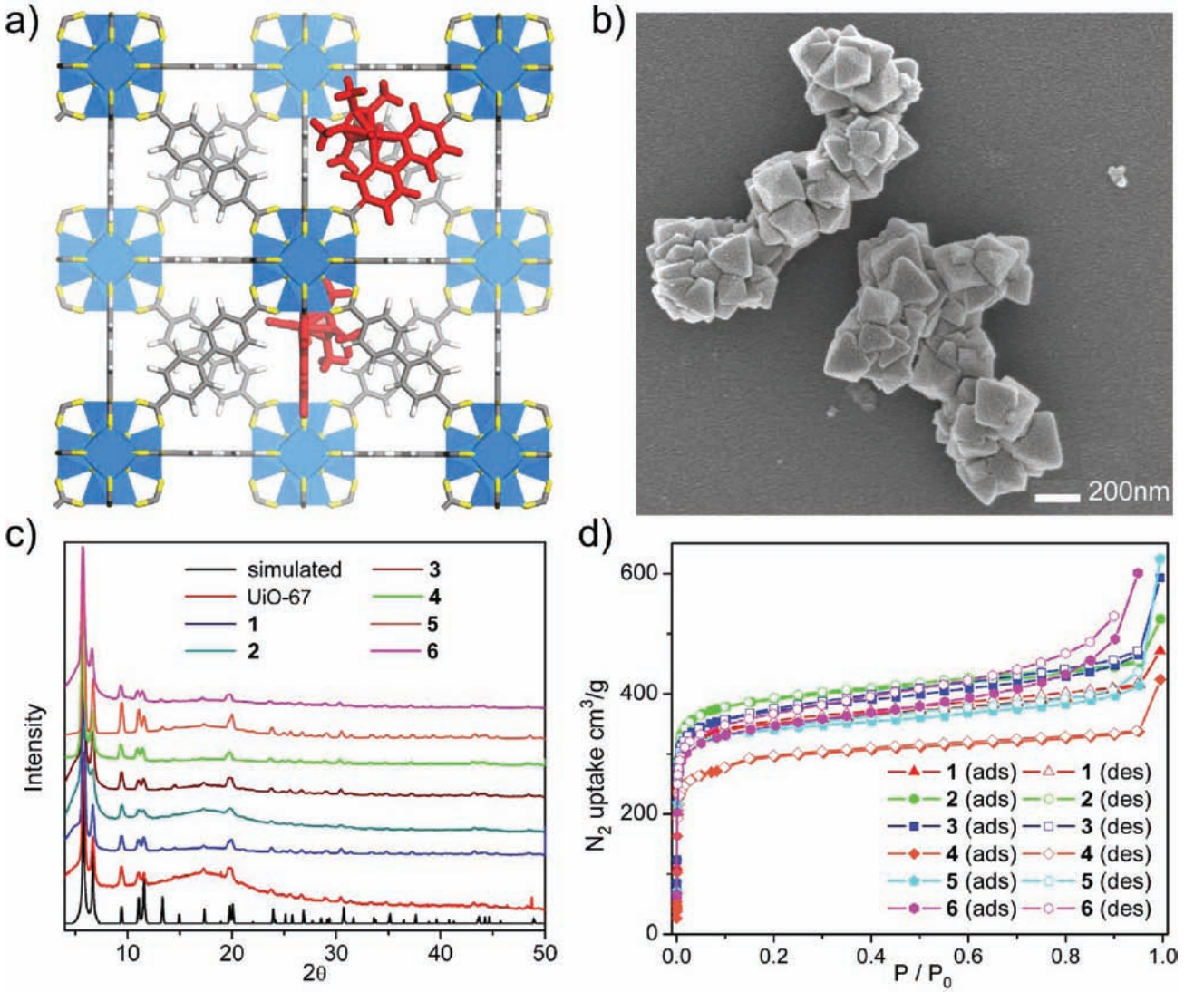

Figure 1. (a) Structure model of MOF-**1** showing doping of the $\mathbf{L_1}$ ligand into the UiO-67 framework. (b) SEM micrograph of intergrown nanocrystals of MOF-**1**. (c) PXRD patterns for UiO-67 and MOFs **1**−**6**. (d) Nitrogen adsorption isotherms of MOFs **1**−**6** at 77 K.

highly active heterogeneous catalysts for photochemical aza-Henry reactions between tertiary amines and nitroalkanes, aerobic amine coupling, and sulfide photo-oxidations.

EXPERIMENTAL SECTION

Detailed experimental procedures can be found in the Supporting Information.

RESULTS AND DISCUSSION

Synthesis of Metal Complex Derivatized MOFs by Doping the UiO-67 Framework. The Ir complexes [IrCp*Cl(dcppy)] ($H_2\mathbf{L_1}$) and [IrCp*Cl(dcbpy)]Cl ($H_2\mathbf{L_2}$) were synthesized by allowing $[IrCp^*Cl_2]_2$ to react with 5,4′-$(EtO_2C)_2$-ppy or 4,4′-$(EtO_2C)_2$-bpy, followed by base-catalyzed hydrolysis. The complex $[Ir(dcppy)_2(H_2O)_2](OTf)$ ($H_2\mathbf{L_3}$) was synthesized by treating $[Ir(dcppy)_2]_2Cl_2$ with AgOTf. The Re complex $[Re(CO)_3(dcbpy)Cl]$ ($H_2\mathbf{L_4}$) was synthesized by a reaction between (2,2′-bipyridine)-5,5′-dicarboxylic acid and pentacarbonylchloro rhenium(I). The Ir complex $[Ir(ppy)_2(dcbpy)]Cl$ ($H_2\mathbf{L_5}$) was synthesized by allowing $[IrCl(ppy)_2]_2$ to react with 4,4′-$(EtO_2C)_2$-bpy, followed by base-catalyzed hydrolysis. The Ru complex $[Ru(bpy)_2(dcbpy)]Cl_2$ ($H_2\mathbf{L_6}$) was synthesized by reacting (2,2′-bipyridine)-5,5′-dicarboxylic acid with $Ru(bpy)_2Cl_2$. Complexes $H_2\mathbf{L_1}$−$H_2\mathbf{L_6}$ were characterized by NMR spectroscopy, and the new compounds $H_2\mathbf{L_1}$, $H_2\mathbf{L_3}$, and $H_2\mathbf{L_5}$ were also characterized by mass spectrometry.

Reactions of $ZrCl_4$ and metal complexes $H_2\mathbf{L_1}$−$H_2\mathbf{L_6}$ in *N*,*N*′-dimethylformamide (DMF) failed to produce crystalline UiO frameworks, presumably due to the steric demand of the $\mathbf{L_1}$−$\mathbf{L_6}$ ligands. Structure modeling studies indicated that the steric bulk of the $\mathbf{L_1}$−$\mathbf{L_6}$ ligands precluded the formation of UiO frameworks based on $Zr_6O_4(OH)_4(CO_2)_{12}$ SBUs and pure $\mathbf{L_1}$−$\mathbf{L_6}$ ligands. We hypothesized that the $\mathbf{L_1}$−$\mathbf{L_6}$ ligands could instead be doped into the framework of UiO-67 ($Zr_6(\mu_3\text{-}O)_4(\mu_3\text{−}OH)_4(bpdc)_6$) by taking advantage of matching ligand lengths between bpdc and $\mathbf{L_1}$−$\mathbf{L_6}$. Such a substitution strategy not only can allow for the incorporation of a sterically demanding bridging ligand into a parent framework but also allows for

retention of the porosity of the parent framework to facilitate substrate diffusion for efficient catalysis.

Metal complex doped UiO-67 (MOFs **1**−**6**) with the $Zr_6(\mu_3\text{-}O)_4(\mu_3\text{-}OH)_4(bpdc)_{6-x}(\mathbf{L})_x$ formula were synthesized by treating $ZrCl_4$ with a combination of H_2bpdc and ligands $H_2\mathbf{L_1}$−$H_2\mathbf{L_6}$ in DMF at 100 °C (Scheme 1). Crystallinity of the MOFs could be enhanced by adding acetic acid to the reaction mixture, which presumably stabilized soluble Zr^{4+} species by acetate coordination and slowed down the formation of amorphous zirconium oxides/hydroxides. Synthetic conditions were optimized to obtain highly crystalline powdery samples of MOFs **1**−**6** (Supporting Information [SI]), which are isostructural with the parent framework UiO-67, based on the similarity of their powder X-ray diffraction (PXRD) patterns (Figures 1a and 1c). SEM images of the samples showed intergrown nanocrystals of ∼200 nm in dimensions (Figure 1b and Figure S3 [SI]). Metal complex contents in MOFs **1**−**6** were established by inductively coupled plasma mass spectrometry (ICP-MS) analysis. MOFs **1**−**6** were found to contain 2−8 wt % of the $\mathbf{L_1}$−$\mathbf{L_6}$ ligands (Table 1). The formulas $Zr_6(\mu_3\text{-}O)_4(\mu_3\text{-}OH)_4(bpdc)_{6-x}(\mathbf{L})_x$ of MOFs **1**−**6** were supported by thermogravimetric analysis (TGA), showing 61−63% weight loss for the organic linkers (Figure S4 [SI]). Permanent porosities of MOFs **1**−**6** were demonstrated by N_2 adsorption at 77 K (Figure 1d). Type I isotherms were obtained for all of the six MOFs with BET surface areas ranging from 1092 to 1497 m^2/g, indicating microporous structures (Table 1). Pore size distribution (calculated by the HK method) centering at 6.7 Å perfectly agrees with that of the structure model (Figure S5 [SI]).

Table 1. Ligand Doping Level and BET Surface Area of MOFs 1−6

MOF x	$\mathbf{L}_x$ ligand wt %[a]	BET surface area (m^2/g)[b]
1	7.7	1254
2	8.1	1497
3	6.0	1410
4	4.2	1092
5	2.0	1194
6	3.0	1277

[a] Determined by ICP-MS. [b] BET surface area calculations were based on the adsorption isotherms using P/P_0 from 0.005 to 0.1.

Water Oxidation Catalysis Using MOFs 1−3. Water oxidation catalytic activities of MOFs **1**−**3** were examined with Ce^{4+} (cerium ammonium nitrate, CAN) as an oxidant (Figure 2a). As shown in Table 2, MOFs **1**−**3** are highly effective water oxidation catalysts with turnover frequencies (TOFs) as high as 4.8 h^{-1}. The catalytic activity must come from the doped $\mathbf{L_1}$−$\mathbf{L_3}$ since the parent UiO-67 did not catalyze water oxidation. The heterogeneous nature of MOFs **1**−**3** was verified by the reusability of MOFs **1**−**3** for water oxidation (Figure 2b) and the lack of catalytic activity for the supernatants of the water oxidation mixtures (Figure 2c), which contained no Ir as determined by ICP-MS. Furthermore, the solids recovered from the reactions exhibited the same PXRD patterns as those of the pristine MOFs **1**−**3** (Figure 2d), supporting the stability of the UiO-67 framework under the present water oxidation conditions.

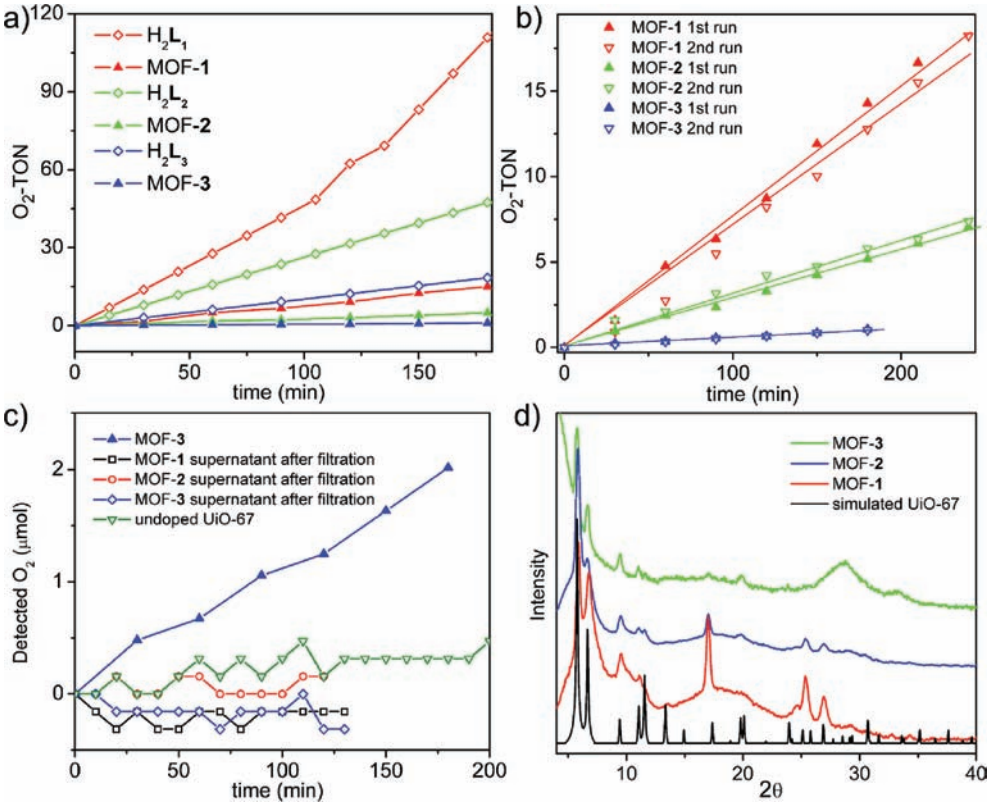

Figure 2. (a) Plots of O_2 evolving turnover number (O_2-TON) vs time for MOFs **1**−**3** and the homogeneous $H_2\mathbf{L_1}$−$H_2\mathbf{L_3}$. (b) Plots of O_2-TON vs time for reuse experiments of MOFs **1**−**3**. (c) The amount of detected O_2 vs time with undoped UiO-67 and supernatant solutions of MOFs **1**−**3** reaction mixtures. The amount of O_2 generated by MOF **3** was also plotted for comparison. (d) PXRD patterns of MOFs **1**−**3** after catalytic reaction and that simulated from the UiO-67 structure.

Table 2. TOFs for MOFs 1−3 Catalyzed Water Oxidation[a]

catalyst	TOF (h^{-1})	catalyst	TOF (h^{-1})
MOF **1**[b]	4.8	H_2L_1[c]	37.0
MOF **2**[b]	1.9	H_2L_2[c]	15.7
MOF **3**[b]	0.4	H_2L_3[c]	6.2

[a] TOF is defined as the number of evolved oxygen molecules per catalytic site per hour over the first 3 h. CAN concentration 62.3−67.1 mM, pH = 1. [b] Heterogeneous catalysis was carried out with 3.2−7.4 mg of MOFs **1**−**3** (equivalent to 0.5−1.0 μmol of Ir WOCs). TOFs were calculated based on the Ir complex doping levels determined by ICP-MS. [c] Homogeneous catalysis with H_2L_1−H_2L_3 was carried out with 1.5−7.5 × 10^{-5} M catalyst.

Table 3. Investigations of MOF 4 as a Photocatalyst for Light-Driven CO_2 Production[a]

entry	photocatalyst	reaction time (h)	H_2-TON[b]	CO-TON[c]
1	MOF **4**	6	0.5	5.0
2 (reuse1)[d]	MOF **4**	6	0.5	6.9
3 (reuse2)[d]	MOF **4**	6	0.6	0
4	supernatant after MOF filtration	6	0.1	0
5	MOF **4**	20	2.5	10.9
6	L_4	6	0.5	2.5
7 (reuse1)[e]	L_4	6	0.8	0.07
8 (reuse2)[f]	L_4	6	0.1	0
9	L_4	20	0.6	3.5
10	$Re(CO)_3Cl(bpy)$	6	0.3	5.6
11	$Re(CO)_3Cl(bpy)$	20	1.0	7.0
12[g]	MOF **4**	6	0.02	0
13[h]	MOF **4**	6	0	0
14	undoped UiO-67	6	0	0

[a] The reaction vials were placed 10 cm in front of a 450 W Xe-lamp with a 300 nm cutoff filter, with magnetic stirring. [b] H_2-TON is defined as the number of evolved hydrogen molecules per catalytic site. [c] CO-TON is defined as the number of evolved CO molecules per catalytic site. [d] The MOF solids were recovered by centrifugation for reuse in new catalytic runs. [e] The reaction solution was degassed with CO_2 before a second photocatalytic run. [f] 100 μL of TEA was added to the reaction solution, and the solution was then degassed with CO_2 before a third photocatalytic run. [g] Without CO_2 [h] Without light.

Comparisons of water oxidation TOFs for MOFs **1**−**3** to those of corresponding homogeneous catalysts H_2L_1−H_2L_3 provide important insights into the reaction processes. MOFs gave lower TOFs than their homogeneous counterparts (only 6.4−12.9% of the homogeneous catalyst activities, Table 2). This level of activity can be accounted for by the Ir catalysts on the MOF particle surface. CAN is apparently too large (~11.3 Å in diameter for the cerium nitrate anions from the crystal structure of CAN) to enter the MOF channels (~6.7 Å in diameter).

A surface poisoning experiment was performed to shed light on the low activity of the MOF catalysts. We first found that treatment of the homogeneous [Ir(Cp*)(ppy)Cl] catalyst with triphenylphosphine (PPh_3) effectively shut down the WOC activity. We isolated the new Ir complex [Ir(Cp*)(ppy)-(PPh_3)]Cl by treating [Ir(Cp*)(ppy)Cl] with triphenylphosphine in ethylacetate at rt for 6 h. The [Ir(Cp*)(ppy)(PPh_3)]Cl complex was an inactive WOC, exhibiting a negligible WOC activity of less than 1/30 of that of the parent [Ir(Cp*)(ppy)Cl] complex (Figure S7 [SI]). The coordination of PPh_3 apparently prevents the water coordination to the Ir center which is key to the water oxidation reaction. We then proceeded to carry out the poisoning experiment on MOF **1** with PPh_3. After being treated with PPh_3, MOF **1** completely lost its WOC activity (Figure S8 [SI]). Considering the much larger size of PPh_3 than the pore size of the MOF **1**, the PPh_3 molecules can only have access to the Ir sites near the surface of the MOF particles, leading to selective surface poisoning of the WOC. The complete shutdown of the WOC activity can only occur if the Ce^{4+}-driven water oxidation reactions exclusively take place near the surface of the MOF particles. This set of control experiments thus unambiguously demonstrated that the MOF catalysts exhibit a lower WOC activity than the homogeneous counterparts due to the inability of the CAN molecules to enter the MOF channels.

Total WOC turnover numbers of MOFs **1**−**3** were determined from UV−vis absorption of the residual Ce^{4+} ions after water oxidation reactions of 12 days. The oxygen sensor can accurately detect O_2 in the gas phase only for a few hours and is not suitable for the longer time-scale experiments. A control experiment using the undoped UiO-67 MOF in the 12-day reactions showed no significant change of the concentration of Ce^{4+}, confirming the validity of this method. The TONs were estimated to be 1513, 1312, and 2152 for MOFs **1**−**3**, respectively.

We do not believe that the water oxidation activity of MOFs **1**−**3** comes from IrO_2 nanoparticles that could result from the decomposition of H_2L_1−H_2L_3. Control experiments using pre-synthesized IrO_2 nanoparticles under the same conditions used with the MOFs indicated that the IrO_2 nanoparticles were a highly active WOC with a TOF of ~150 h^{-1}. However, the IrO_2 nanoparticles were unstable under the reaction conditions with their catalytic activity lasting for less than 30 min. The addition of more Ce^{4+} to the reaction mixture did not produce more O_2. The facts that the MOF catalysts could be reused and MOFs **1**−**3** each exhibited different water oxidation activity also argue against the possibility that in situ generated IrO_2 nanoparticles are responsible for water oxidation. The complete poisoning of MOF **1** by PPh_3 also supported the molecular origin of the WOC activity in the MOFs. X-ray photoelectron spectroscopic analyses of the fresh and recovered MOFs were inconclusive, as the Ir 4f binding energies of the L_1−L_3 ligands were too close to those of IrO_2 (Figure S6 [SI]).

Photocatalytic CO_2 Reduction Using MOF 4. The Re-based L_4 ligand can serve as an active catalyst for photochemical CO_2 reduction. Photocatalytic CO_2 reduction activity of MOF **4** was examined in CO_2-saturated acetonitrile (MeCN), using triethylamine (TEA) as a sacrificial reducing agent. Immediately after irradiating the reaction mixture, the MOF **4** color changed from orange to green, suggestive of catalytic turnovers. As shown in Table 3, the MOF catalyst selectively reduced CO_2 to CO under light, as determined by gas chromatography (GC). Under the reaction conditions (MeCN/TEA = 20/1, regular MeCN and TEA, saturated with CO_2 gas), the molar ratio of the CO and H_2 production was around 10 during the first six hours. When the photocatalytic CO_2 reduction was carried out with CD_3CN as the solvent, no formic acid or methanol product was detected by ^1H NMR spectroscopy. The CO-TONs reached 5.0 after the first six hours (Table 3, entry 1). No CO generation was observed in the absence of CO_2 under the same reaction conditions (Table 3, entry 12), ruling out the possibility that the detected CO could

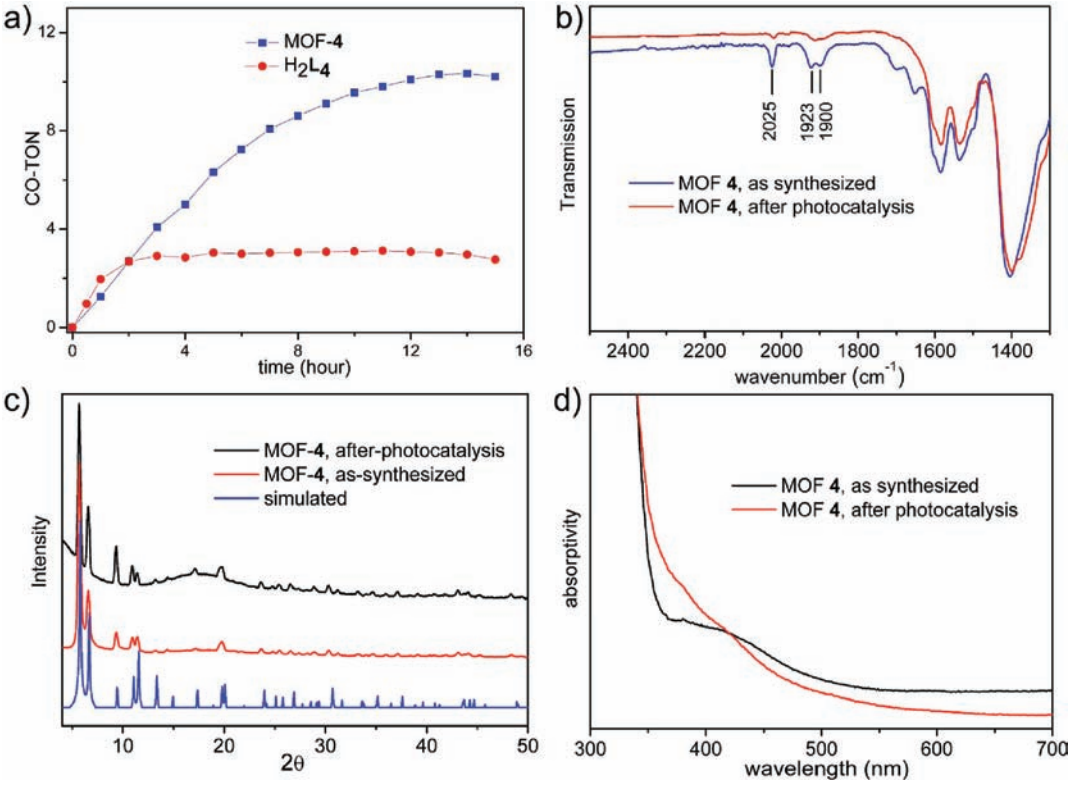

Figure 3. (a) Plots of CO evolution turnover number (CO-TON) versus time in the photocatalytic CO_2 reduction with MOF **4** (blue square) and homogeneous H_2L_4 (red circle). (b) FT-IR of as-synthesized MOF **4** (blue) and MOF **4** after photocatalysis (red). (c) PXRD patterns of MOF **4** after catalysis (black), as-synthesized (red), and simulated from the UiO-67 structure (blue). (d) UV−vis diffuse reflectance spectra of as-synthesized MOF **4** (black) and MOF **4** after photocatalysis (red).

have resulted from the decomposition of the L_4 ligand. The photocatalytic nature of the reaction was proved by the fact that no CO was generated in the dark (Table 3, entry 13). The inactivity of the parent UiO-67 framework in this reaction confirmed that the $[Re^I(dcbpy)(CO)_3Cl]$ moiety was responsible for the catalytic CO_2 reduction (Table 3, entry 14).

We also tested the recyclability of the MOF **4** catalyst in light-driven CO_2 reduction. The solid in the reaction mixture was recovered via centrifugation and reused in additional runs of catalytic reactions. However, after two six-hour reaction runs, the catalyst became inactive in CO generation, but a small amount of H_2 was still detected (Table 3, entries 2 and 3). The supernatant of the MOF **4** reaction mixture showed no CO generation activity but slight H_2 generation activity (Table 3, entry 4). The total CO-TON of the MOF **4** catalyst was estimated to be 10.9 from the 20 h reaction (Table 3, entry 5). During the 20 h reaction, 43.6% of the Re had leached into the supernatant, as determined by ICP-MS. In contrast, only 3.5% of the Zr was detected in the supernatant by ICP-MS. PXRD of the recovered solid indicated that the framework structure of MOF **4** remained intact (Figure 3c). These results suggest that the Re leached into solution via the detachment of Re-carbonyl moieties from the dcbpy group in the MOF **4** framework and not by MOF **4** dissolution. Consistent with this, the recovered MOF **4** lost the UV−vis peak at 412 nm that is characteristic of the ^{1}MLCT absorption of the $Re(CO)_3(bpy)Cl$ species (Figure 3d). The intensities of the IR peaks corresponding to the CO stretching vibrations of the L_4 ligand at ~2025 cm^{-1}(A′), ~1923 cm^{-1}(A′), and ~1900 cm^{-1} (A″) significantly decreased in the recovered solid when compared to those of the as-synthesized MOF **4** (Figure 3b), further supporting the decomposition of the L_4 ligand by losing the Re-carbonyl moieties.

Photocatalytic CO_2 reduction was also conducted with the homogeneous ligand L_4 under the same conditions. Upon irradiation, the reaction mixture also turned from orange to green color immediately. After a six hour reaction, the solution color turned to yellowish gray, and GC analysis indicated a moderate CO-TON of 2.5 (Table 3, entry 6). The reaction mixture was almost inactive in the second photocatalytic run, even after resaturating the solution with CO_2 (Table 3, entry 7). Adding more TEA to the solution did not regenerate the catalytic activity (Table 3, entry 8). All of these observations indicated that the Re L_4 ligand decomposed during the catalytic turnovers. The overall CO-TON for the homogeneous H_2L_4 ligand was estimated to be 3.5 based on the 20 h reaction (Table 3, entry 9). A time-dependent catalytic activity experiment was performed by analyzing the CO production at different time points by GC (Figure 3a). Although the homogeneous H_2L_4 was more active than the MOF **4** catalyst in the first two hours, the MOF **4** catalyst retained activity over a longer reaction time to yield a higher total TON. The MOF **4** catalyst thus exhibited much higher total TONs than the homogeneous system, presumably as a result of the catalyst stabilization by the MOF framework. Reactions using $Re(CO)_3(bpy)Cl$ as catalyst were performed to test our experimental setup and reaction conditions (Table 3, entries 10 and 11). A total TON of 7.0 was obtained after 20 h of irradiation, which is comparable to the previously reported value.[69]

Table 4. MOF 5 and MOF 6 Catalyzed aza-Henry Reactions[a]

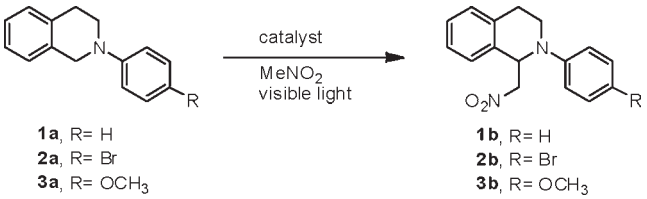

1a, R= H
2a, R= Br
3a, R= OCH_3

1b, R= H
2b, R= Br
3b, R= OCH_3

		catalyst/conv. (%)[b]				
entry	substrate	no catalyst	MOF **5**	L_5-Et_2[c]	MOF **6**	L_6-Et_2[c]
1	**1a**	19	59	99	86	97
2	**2a**	17	62	90	68	88
3	**3a**	28	96	>99	97	>99

[a] The reactions were carried out with 1 mol % catalyst loading, 5 cm in front of a 26 W fluorescent lamp for 12 h. [b] Conversion yields were determined by ^{1}H NMR. [c] As the H_2L_5 acid ligand has very low solubility in nitromethane, the diethyl esters of L_5 and L_6 ligands L_5-Et_2 and L_6-Et_2 were used in the homogeneous control experiments instead.

Previous mechanistic studies on the $[Re(CO)_3(bpy)Cl]$-catalyzed CO_2 reduction suggested both a unimolecular pathway involving a $[Re^I(bpy)(CO)_3(COOH)]$ intermediate[83] and a bimolecular pathway involving a CO_2-bridged Re dimer $[(CO)_3(bpy)Re^I](CO_2)[Re^I(bpy)(CO)_3]$[84,85] or outer-sphere redox reactions between two Re molecules[69] in the catalytic cycle. The present MOF **4** catalyzed CO_2 reduction can only occur via the unimolecular mechanism as a result of the immobilization of the L_4 catalyst in the MOF framework. Interestingly, the incorporation of L_4 into the MOF **4** framework not only led to higher CO_2 reduction TONs but also shed light on the CO_2 reduction reaction mechanisms and photocatalyst decomposition pathways.

Photocatalytic Organic Transformations using MOF 5 and MOF 6. Catalytic activities of $Ir(ppy)_2(bpy)^+$-based MOF **5** and $Ru(bpy)_3^{2+}$-based MOF **6** toward photocatalytic aza-Henry reactions were evaluated with tetrahydroisoquinoline (**1a**) as the amine substrate and CH_3NO_2 as solvent. The reaction was carried out in the presence of air with a common fluorescent lamp (26 W) as the light source. The reaction was stopped after 12 h, and the MOF catalysts were filtered off. Conversions of the reactions were determined by integrating the peaks of ^{1}H NMR spectra of the crude reaction mixtures (SI). As shown in Table 4 (entry 1), both MOF **5** and MOF **6** were highly effective photocatalysts for the aza-Henry reaction between **1a** and nitromethane, with 59% and 86% conversions, respectively. The MOF **5** and MOF **6** catalysts also effectively catalyzed the aza-Henry reactions between nitromethane and bromo- and methoxy-substituted tetrahydroisoquinoline (**2a** and **3a**) with high efficiency (Table 4, entries 2 and 3). A number of control experiments were carried out to demonstrate the heterogeneous and photocatalytic nature of the reactions. The reaction of **1a** in the dark yielded negligible amounts of aza-Henry products (<5%), demonstrating the necessity of light in this reaction. On the other hand, the background reaction in the absence of the catalysts but in the presence of light showed only 19% conversion after 12 h (Table 4, entry 1), indicating that the MOF played a catalytic role in the reactions. These observations are consistent with those of the homogeneous catalytic system reported by Stephenson and co-workers.[74] In addition, a crossover

Table 5. Reuse of MOF 5 and MOF 6 in aza-Henry reactions[a]

		conv. (%)[b]		
catalyst	substrate	1st run	2nd run	3rd run
MOF-**5**	**1a**	59	57	59
MOF-**5**	**2a**	62	68	68
MOF-**5**	**3a**	96	93	95
MOF-**6**	**1a**	86	69	62
MOF-**6**	**2a**	68	71	66
MOF-**6**	**3a**	97	93	95

[a] The reactions were carried out with 1 mol % catalyst loading, 5 cm in front of a 26 W fluorescent lamp for 12 h. [b] Conversion yields were determined by ^{1}H NMR.

experiment was carried out to prove the heterogeneity of the MOF catalyst. Substrate **3a** was first used in the MOF **6** catalyzed aza-Henry reaction, and 95% conversion was achieved after 12 h. The MOF catalyst was then removed by filtering through Celite, and another substrate **1a** was added to the supernatant solution. After stirring the solution under light for 12 h, only 22% conversion was observed for the second substrate. This low conversion, comparable to that of the background reaction, proved that the supernatant of the MOF **6** reaction mixture is inactive in photocatalysis, supporting the heterogeneous nature of the MOF photocatalysts. A further examination of the supernatant by ICP-MS showed no observable leaching of Ru to the solution during the reaction. The MOF **5** and **6** catalysts were also recovered from the reaction mixture by centrifugation and reused three times without loss of activity (Table 5). In addition, PXRD patterns of MOF **5** and **6** after the reactions showed no deterioration of the crystallinity (Figure 4).

We performed another control experiment to demonstrate the need of MOF permanent porosity in catalyzing the photo-driven aza-Henry reaction. Amorphous nanoparticles were synthesized under conditions similar to those of MOF **6** except that wet DMF was used in the synthesis and glacial acetic acid was not added. The resultant material was nonporous as indicated by N_2 adsorption measurement (with a negligible BET surface area of 46 m^2/g, Figure S19 [SI]) and amorphous by PXRD (Figure S20 [SI]). The L_6 ligand weight percentage in this material was found to be higher than that of MOF **6** by ICP-MS measurements (7.0 wt %). However, the nonporous nanoparticles did not catalyze the aza-Henry reaction using **1a** as the substrate (18% conversion, corresponding to background reaction) at the same catalyst loading as MOF **6**. This observation unambiguously supported that the photoredox step of the reaction happened inside the channels of MOF **5** and MOF **6**. Although the substrate amines are relatively large compared to the size of channels in these MOFs, it is still possible for them to move through the MOF channels as a result of favorable interactions between the amine substrates and the MOF framework (e.g., $\pi-\pi$ stacking interactions).[86] Alternatively, it is possible that the aza-Henry reaction can be mediated by photochemically generated singlet oxygen,[87] which will allow the photocatalysis with substrates much larger than the open channels since only O_2 molecules need to diffuse through the MOF channels. As surface photocatalytic sites of these systems have minor contributions to the overall photocatalysis (<12% as indicated by the water oxidation activity shown above), microporosity is a prerequisite for the high activity of these doped MOFs.

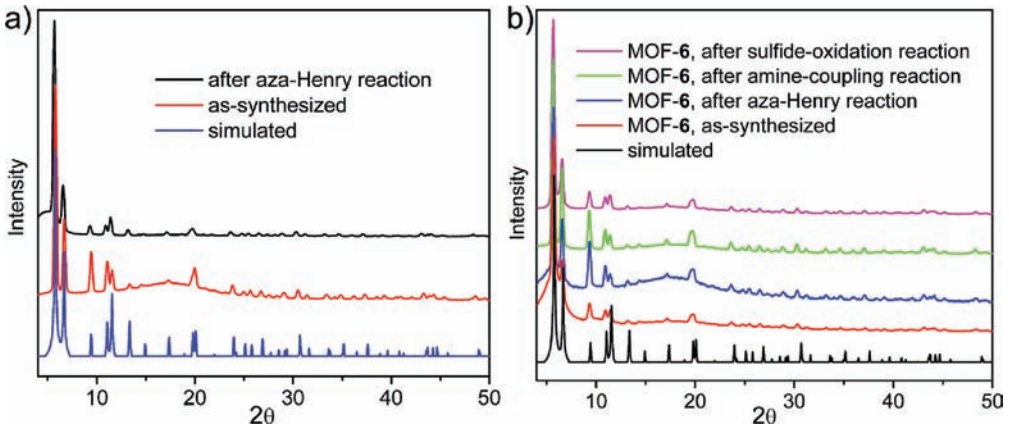

Figure 4. (a) PXRD patterns of MOF **5**: as-synthesized (red), after aza-Henry reaction (black), and simulated from the UiO-67 structure (blue). (b) PXRD patterns of MOF **6**: after sulfide oxidation (pink), after amine coupling (green), after aza-Henry reaction (blue), as-synthesized (red), and simulated from the UiO-67 structure (black).

Table 6. Photocatalytic Aerobic Amine Coupling Reactions[a]

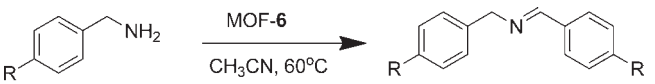

1c : R = H
2c : R = Me
3c : R = OMe

1d : R = H
2d : R = Me
3d : R = OMe

entry	catalyst	substrate	yield %[b]
1	MOF **6**	**1c**	83
2	MOF **6** (reuse)	**1c**	80
3	L_6	**1c**	96
4	no catalyst	**1c**	8
5[c]	MOF **6**	**1c**	6
6	MOF **6**	**2c**	90
7	MOF **6**	**3c**	46

[a] Reactions were carried out with 1 mol % catalyst loadings, 5 cm in front of a 300 W Xe lamp for 1 h. [b] Yields were determined by ^{1}H NMR based on the product/[product + starting material] ratio. [c] Without light.

We also demonstrated the applicability of the $Ru(bpy)_3^{2+}$-based MOF **6** as a photocatalyst in other light-driven reactions. As shown in Table 6, MOF **6** efficiently catalyzed aerobic oxidative coupling of a series of primary amines with 46−90% conversions in three hours (Table 6, entries 1, 6, and 7). The conversion of substrate **1c** using the MOF **6** was comparable to that using the homogeneous molecular catalyst (Table 6, entry 3). The recyclability and reusability of MOF **6** were also evaluated in this reaction using **1c** as the substrate. The recovered catalyst from simple filtration showed no deterioration of conversion % (Table 6, entry 2) and retained the crystallinity of the pristine sample (Figure 4b). The background reaction in the absence of the catalyst but in the presence of light showed only ~8% conversion (Table 6, entry 4), verifying that MOF **6** played a catalytic role in the reactions. On the other hand, the reaction of **1c** in the dark yielded negligible amounts of coupling products (Table 6, entry 5), demonstrating the necessity of light in this reaction. These observations are consistent with those reported by Lang et al.[75] and Su et al.[76] using carbon nitride and TiO_2 as photocatalysts. Time-dependent conversions of the three substrates have also been monitored by GC analysis at different time points, which gave similar initial reaction rates for the three different substrates. The absence of size selectivity of the initial reaction rates is consistent with the singlet oxygen-mediated reaction mechanism. The seemingly lower finial yield of **3d** is due to its slow decomposition on MOF **6**, presumably catalyzed by the Lewis acidic $[Zr_6(\mu_3\text{-}O)_4(\mu_3\text{-}OH)_4(CO_2)_{12}]$ building block.

Table 7. Photo-Oxidation of Thioanisole

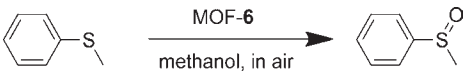

entry	catalyst/reaction condition	time (h)	conversion %
1	L_6	22	72
2	MOF-**6**	22	73
3	no catalyst, with light	22	0
4	no light, with L_6	22	0
5	no light, with MOF **6**	22	0
6	L_6 under N_2 protection	22	0
7	MOF **6**, under N_2 protection	22	0

The photocatalyzed aerobic oxidation of thioanisole was also examined, using MOF **6** as the photocatalyst. Photocatalytic aerobic oxidation of sulfide to sulfoxide has been reported before with $Ru(bpy)_3^{2+}$ in acetonitrile but only when a lead ruthenate pyrochlore mineral was added as an electron shuttle.[77] We found that by changing the solvent to methanol the photocatalyzed sulfide oxidation occurred without an electron relay (Table 7, entry 1). It is highly likely that the thioanisole oxidation reaction is mediated by the photochemically generated singlet oxygen.[88−90] As shown in Table 7, with methanol as the solvent, MOF **6** catalyzed the selective aerobic oxidation of thioanisole to methyl phenyl sulfoxide. No sulfone (the possible overoxidized byproduct) was detected by ^{1}H NMR, demonstrating a high degree of selectivity of this reaction. The conversion % after 22 h is comparable to that of the corresponding homogeneous catalytic system (Table 7, entries 1 and 2). A control experiment with no photocatalyst but with light showed no appreciable conversion of the sulfide

(Table 7, entry 3). No sulfoxide products were detected when the reactions were carried out in the absence of light but in the presence of MOF **6** or $\mathbf{L_6}$ (Table 7, entries 4 and 5). O_2 was shown to be the oxidizing agent since no conversion of sulfide to sulfoxide was observed when the reaction was carried out under N_2 protection (Table 7, entries 6 and 7). The PXRD pattern of the MOF **6** catalyst after the reaction was identical to that of the pristine MOF **6**, indicating its stability under the reaction conditions (Figure 4).

CONCLUSIONS

We have successfully incorporated Ir, Re, and Ru complexes into the UiO framework by a mix-and-match strategy. These stable and porous metal complex-derivatized doped MOFs are highly effective catalysts for a range of reactions related to solar energy utilization. MOFs **1**−**3** were used in catalytic water oxidation, while MOF **4** catalyzed photochemical CO_2 reduction. MOFs **5** and **6** were used in three photocatalytic organic tranformations: aza-Henry reaction, aerobic amine coupling, and aerobic thioanisole oxidation. Stability of these MOF catalysts under the reaction conditions was verified by comparing PXRD patterns before and after catalysis. The heterogeneous nature of these catalysts can not only facilitate catalyst recycling and reuse but also provide mechanistic insights into the reactions, as in the case of CO_2 reduction using MOF **4**. The modular nature of this synthetic approach should allow further fine tuning and optimization to lead to highly active heterogeneous catalysts in solar energy utilization.

ASSOCIATED CONTENT

Supporting Information. Detailed experimental procedures and characterization data. This material is available free of charge via the Internet at http://pubs.acs.org.

AUTHOR INFORMATION

Corresponding Author
wlin@unc.edu

ACKNOWLEDGMENT

We acknowledge sole financial support from the UNC EFRC: Solar Fuels and Next Generation Photovoltaics, and Energy Frontier Research Center funded by the U.S. Department of Energy, Office of Science, Office of Basic Energy Sciences (DE-SC0001011).

REFERENCES

(1) Hammarström, L.; Hammes-Schiffer, S. *Acc. Chem. Res.* **2009**, *42*, 1859.
(2) Ciamician, G. *Science* **1912**, *36*, 385.
(3) Fujishima, A.; Honda, K. *Nature* **1972**, *238*, 37.
(4) Gust, D.; Moore, T. A.; Moore, A. L. *Acc. Chem. Res.* **2009**, *42*, 1890.
(5) Concepcion, J. J.; Jurss, J. W.; Brennaman, M. K.; Hoertz, P. G.; Patrocinio, A. O. v. T.; Murakami Iha, N. Y.; Templeton, J. L.; Meyer, T. J. *Acc. Chem. Res.* **2009**, *42*, 1954.
(6) Esswein, M. J.; Nocera, D. G. *Chem. Rev.* **2007**, *107*, 4022.
(7) Dubois, M. R.; Dubois, D. L. *Acc. Chem. Res.* **2009**, *42*, 1974.
(8) Morris, A. J.; Meyer, G. J.; Fujita, E. *Acc. Chem. Res.* **2009**, *42*, 1983.
(9) Narayanam, J. M. R.; Stephenson, C. R. J. *Chem. Soc. Rev.* **2011**, *40*, 102.
(10) Wasielewski, M. R. *Acc. Chem. Res.* **2009**, *42*, 1910.
(11) Ferey, G.; Mellot-Draznieks, C.; Serre, C.; Millange, F. *Acc. Chem. Res.* **2005**, *38*, 217.
(12) Kitagawa, S.; Kitaura, R.; Noro, S. *Angew. Chem., Int. Ed.* **2004**, *43*, 2334.
(13) Long, J. R.; Yaghi, O. M. *Chem. Soc. Rev.* **2009**, *38*, 1213.
(14) Farha, O. K.; Hupp, J. T. *Acc. Chem. Res.* **2010**, *43*, 1166.
(15) Tanabe, K. K.; Cohen, S. M. *Chem. Soc. Rev.* **2011**, *40*, 498.
(16) Eddaoudi, M.; Kim, J.; Rosi, N.; Vodak, D.; Wachter, J.; O'Keeffe, M.; Yaghi, O. M. *Science* **2002**, *295*, 469.
(17) Murray, L. J.; Dinca, M.; Long, J. R. *Chem. Soc. Rev.* **2009**, *38*, 1294.
(18) Li, J. R.; Kuppler, R. J.; Zhou, H. C. *Chem. Soc. Rev.* **2009**, *38*, 1477.
(19) Xiang, S.-C.; Zhang, Z.; Zhao, C.-G.; Hong, K.; Zhao, X.; Ding, D.-R.; Xie, M.-H.; Wu, C.-D.; Das, M. C.; Gill, R.; Thomas, K. M.; Chen, B. *Nat. Commun.* **2011**, *2*, 204.
(20) Allendorf, M. D.; Houk, R. J.; Andruszkiewicz, L.; Talin, A. A.; Pikarsky, J.; Choudhury, A.; Gall, K. A.; Hesketh, P. J. *J. Am. Chem. Soc.* **2008**, *130*, 14404.
(21) Lan, A.; Li, K.; Wu, H.; Olson, D. H.; Emge, T. J.; Ki, W.; Hong, M.; Li, J. *Angew. Chem., Int. Ed.* **2009**, *48*, 2334.
(22) Xie, Z.; Ma, L.; deKrafft, K. E.; Jin, A.; Lin, W. *J. Am. Chem. Soc.* **2010**, *132*, 922.
(23) Lu, G.; Hupp, J. T. *J. Am. Chem. Soc.* **2010**, *132*, 7832.
(24) Evans, O. R.; Lin, W. *Acc. Chem. Res.* **2002**, *35*, 511.
(25) deKrafft, K. E.; Xie, Z.; Cao, G.; Tran, S.; Ma, L.; Zhou, O. Z.; Lin, W. *Angew. Chem., Int. Ed.* **2009**, *48*, 9901.
(26) Della Rocca, J.; Lin, W. B. *Eur. J. Inorg. Chem.* **2010**, *24*, 3725.
(27) Liu, D.; Huxford, R. C.; Lin, W. *Angew. Chem., Int. Ed.* **2011**, *50*, 3696.
(28) Horcajada, P.; Chalati, T.; Serre, C.; Gillet, B.; Sebrie, C.; Baati, T.; Eubank, J. F.; Heurtaux, D.; Clayette, P.; Kreuz, C.; Chang, J. S.; Hwang, Y. K.; Marsaud, V.; Bories, P. N.; Cynober, L.; Gil, S.; Ferey, G.; Couvreur, P.; Gref, R. *Nat. Mater.* **2010**, *9*, 172.
(29) Lin, W.; Rieter, W. J.; Taylor, K. M. *Angew. Chem., Int. Ed.* **2009**, *48*, 650.
(30) Rieter, W. J.; Pott, K. M.; Taylor, K. M.; Lin, W. *J. Am. Chem. Soc.* **2008**, *130*, 11584.
(31) Ma, L.; Abney, C.; Lin, W. *Chem. Soc. Rev.* **2009**, *38*, 1248.
(32) Ma, L. F., J. M.; Abney, C.; Lin, W. *Nat. Chem.* **2010**, *2*, 838.
(33) Song, F.; Wang, C.; Falkowski, J. M.; Ma, L.; Lin, W. *J. Am. Chem. Soc.* **2010**, *132*, 15390.
(34) Cho, S. H.; Ma, B.; Nguyen, S. T.; Hupp, J. T.; Albrecht-Schmitt, T. E. *Chem. Commun.* **2006**, 2563.
(35) Banerjee, M.; Das, S.; Yoon, M.; Choi, H. J.; Hyun, M. H.; Park, S. M.; Seo, G.; Kim, K. *J. Am. Chem. Soc.* **2009**, *131*, 7524.
(36) Kent, C. A.; Mehl, B. P.; Ma, L.; Papanikolas, J. M.; Meyer, T. J.; Lin, W. *J. Am. Chem. Soc.* **2010**, *132*, 12767.
(37) Duan, L.; Fischer, A.; Xu, Y.; Sun, L. *J. Am. Chem. Soc.* **2009**, *131*, 10397.
(38) Zong, R.; Thummel, R. P. *J. Am. Chem. Soc.* **2005**, *127*, 12802.
(39) Concepcion, J. J.; Jurss, J. W.; Templeton, J. L.; Meyer, T. J. *J. Am. Chem. Soc.* **2008**, *130*, 16462.
(40) Tseng, H. W.; Zong, R.; Muckerman, J. T.; Thummel, R. *Inorg. Chem.* **2008**, *47*, 11763.
(41) Ellis, W. C.; McDaniel, N. D.; Bernhard, S.; Collins, T. J. *J. Am. Chem. Soc.* **2010**, *132*, 10990.
(42) McDaniel, N. D.; Coughlin, F. J.; Tinker, L. L.; Bernhard, S. *J. Am. Chem. Soc.* **2008**, *130*, 210.
(43) Hull, J. F.; Balcells, D.; Blakemore, J. D.; Incarvito, C. D.; Eisenstein, O.; Brudvig, G. W.; Crabtree, R. H. *J. Am. Chem. Soc.* **2009**, *131*, 8730.
(44) Blakemore, J. D.; Schley, N. D.; Balcells, D.; Hull, J. F.; Olack, G. W.; Incarvito, C. D.; Eisenstein, O.; Brudvig, G. W.; Crabtree, R. H. *J. Am. Chem. Soc.* **2010**, *132*, 16017.

(45) Geletii, Y. V.; Huang, Z.; Hou, Y.; Musaev, D. G.; Lian, T.; Hill, C. L. *J. Am. Chem. Soc.* **2009**, *131*, 7522.
(46) Yin, Q.; Tan, J. M.; Besson, C.; Geletii, Y. V.; Musaev, D. G.; Kuznetsov, A. E.; Luo, Z.; Hardcastle, K. I.; Hill, C. L. *Science* **2010**, *328*, 342.
(47) Morris, N. D.; Mallouk, T. E. *J. Am. Chem. Soc.* **2002**, *124*, 11114.
(48) Nakagawa, T.; Bjorge, N. S.; Murray, R. W. *J. Am. Chem. Soc.* **2009**, *131*, 15578.
(49) Youngblood, W. J.; Lee, S. H.; Kobayashi, Y.; Hernandez-Pagan, E. A.; Hoertz, P. G.; Moore, T. A.; Moore, A. L.; Gust, D.; Mallouk, T. E. *J. Am. Chem. Soc.* **2009**, *131*, 926.
(50) Jiao, F.; Frei, H. *Angew. Chem., Int. Ed.* **2009**, *48*, 1841.
(51) Kanan, M. W.; Nocera, D. G. *Science* **2008**, *321*, 1072.
(52) Low, J. J.; Benin, A. I.; Jakubczak, P.; Abrahamian, J. F.; Faheem, S. A.; Willis, R. R. *J. Am. Chem. Soc.* **2009**, *131*, 15834.
(53) Cavka, J. H.; Jakobsen, S.; Olsbye, U.; Guillou, N.; Lamberti, C.; Bordiga, S.; Lillerud, K. P. *J. Am. Chem. Soc.* **2008**, *130*, 13850.
(54) Guillerm, V.; Gross, S.; Serre, C.; Devic, T.; Bauer, M.; Ferey, G. *Chem. Commun.* **2010**, *46*, 767.
(55) Jordan, P.; Fromme, P.; Witt, H. T.; Klukas, O.; Saenger, W.; Krausz, N. *Nature* **2001**, *411*, 909.
(56) Tinnemans, A. H. A.; Koster, T. P. M.; Thewissen, D. H. M. W.; Mackor, A. *Recl.: J. R. Neth. Chem. Soc.* **1984**, *103*, 288.
(57) Matsuoka, S.; Yamamoto, K.; Ogata, T.; Kusaba, M.; Nakashima, N.; Fujita, E.; Yanagida, S. *J. Am. Chem. Soc.* **1993**, *115*, 601.
(58) Ogata, T.; Yamamoto, Y.; Wada, Y.; Murakoshi, K.; Kusaba, M.; Nakashima, N.; Ishida, A.; Takamuku, S.; Yanagida, S. *J. Phys. Chem.* **1995**, *99*, 11916.
(59) Beley, M.; Collin, J. P.; Ruppert, R.; Sauvage, J. P. *J. Am. Chem. Soc.* **1986**, *108*, 7461.
(60) Craig, C. A.; Spreer, L. O.; Otvos, J. W.; Calvin, M. *J. Phys. Chem.* **1990**, *94*, 7957.
(61) Behar, D.; Dhanasekaran, T.; Neta, P.; Hosten, C. M.; Ejeh, D.; Hambright, P.; Fujita, E. *J. Phys. Chem. A* **1998**, *102*, 2870.
(62) Grodkowski, J.; Behar, D.; Neta, P.; Hambright, P. *J. Phys. Chem. A* **1997**, *101*, 248.
(63) Grodkowski, J.; Dhanasekaran, T.; Neta, P.; Hambright, P.; Brunschwig, B. S.; Shinozaki, K.; Fujita, E. *J. Phys. Chem. A* **2000**, *104*, 11332.
(64) Grodkowski, J.; Neta, P. *J. Phys. Chem. A* **2000**, *104*, 1848.
(65) Grodkowski, J.; Neta, P.; Fujita, E.; Mahammed, A.; Simkhovich, L.; Gross, Z. *J. Phys. Chem. A* **2002**, *106*, 4772.
(66) Hawecker, J.; Lehn, J. M.; Ziessel, R. *J. Chem. Soc., Chem. Commun.* **1983**, 536.
(67) Hori, H.; Johnson, F. P. A.; Koike, K.; Ishitani, O.; Ibusuki, T. *J. Photochem. Photobiol., A* **1996**, *96*, 171.
(68) Hori, H.; Koike, K.; Suzuki, Y.; Ishizuka, M.; Tanaka, J.; Takeuchi, K.; Sasaki, Y. *J. Mol. Catal. A: Chem.* **2002**, *179*, 1.
(69) Takeda, H.; Koike, K.; Inoue, H.; Ishitani, O. *J. Am. Chem. Soc.* **2008**, *130*, 2023.
(70) Doherty, M. D.; Grills, D. C.; Fujita, E. *Inorg. Chem.* **2009**, *48*, 1796.
(71) Narayanam, J. M.; Stephenson, C. R. *Chem. Soc. Rev.* **2011**, *40*, 102.
(72) Ischay, M. A.; Anzovino, M. E.; Du, J.; Yoon, T. P. *J. Am. Chem. Soc.* **2008**, *130*, 12886.
(73) Narayanam, J. M.; Tucker, J. W.; Stephenson, C. R. *J. Am. Chem. Soc.* **2009**, *131*, 8756.
(74) Condie, A. G.; Gonzalez-Gomez, J. C.; Stephenson, C. R. *J. Am. Chem. Soc.* **2010**, *132*, 1464.
(75) Lang, X.; Ji, H.; Chen, C.; Ma, W.; Zhao, J. *Angew. Chem., Int. Ed.* **2011**, *50*, 3934.
(76) Su, F.; Mathew, S. C.; Mohlmann, L.; Antonietti, M.; Wang, X.; Blechert, S. *Angew. Chem., Int. Ed.* **2011**, *50*, 657.
(77) Zen, J. M.; Liou, S. L.; Kumar, A. S.; Hsia, M. S. *Angew. Chem., Int. Ed.* **2003**, *42*, 577.
(78) Chen, W.; Rein, F. N.; Rocha, R. C. *Angew. Chem., Int. Ed.* **2009**, *48*, 9672.
(79) Fukuzumi, S.; Kishi, T.; Kotani, H.; Lee, Y.-M.; Nam, W. *Nat. Chem.* **2011**, *3*, 38.
(80) Dai, C.; Narayanam, J. M.; Stephenson, C. R. *Nat. Chem.* **2011**, *3*, 140.
(81) Nicewicz, D. A.; MacMillan, D. W. *Science* **2008**, *322*, 77.
(82) Tucker, J. W.; Nguyen, J. D.; Narayanam, J. M.; Krabbe, S. W.; Stephenson, C. R. *Chem. Commun.* **2010**, *46*, 4985.
(83) Gibson, D. H.; Yin, X.; He, H.; Mashuta, M. S. *Organometallics* **2003**, *22*, 337.
(84) Gibson, D. H.; Yin, X. *J. Am. Chem. Soc.* **1998**, *120*, 11200.
(85) Hayashi, Y.; Kita, S.; Brunschwig, B. S.; Fujita, E. *J. Am. Chem. Soc.* **2003**, *125*, 11976.
(86) Wang, C.; Lin, W. *J. Am. Chem. Soc.* **2011**, *133*, 4232.
(87) Jiang, G.; Chen, J.; Huang, J.-S.; Che, C.-M. *Org. Lett.* **2009**, *11*, 4568.
(88) Ferroud, C.; Rool, P.; Santamaria, J. *Tetrahedron Lett.* **1998**, *39*, 9423.
(89) Liang, J. J.; Gu, C. L.; Kacher, M. L.; Foote, C. S. *J. Am. Chem. Soc.* **1983**, *105*, 4717.
(90) Foote, C. S.; Peters, J. W. *J. Am. Chem. Soc.* **1971**, *93*, 3795.